Neuroinflammation in Olfactory Circuits Underlies Odor Hypersensitivity in a Rodent Model of Depression

Kai Clane Belonio[1], Zach Fyke[2], Eyerusalem S. Haile[3], Joseph D. Zak[1,4]

1. Department of Biological Sciences, University of Illinois Chicago, Chicago, IL 60607
2. Graduate Program in Neuroscience, University of Illinois Chicago, Chicago, IL 60607
3. Graduate Program in Biological Sciences, University of Illinois Chicago, Chicago, IL 60607
4. Department of Psychology, University of Illinois Chicago, Chicago, IL 60607

Correspondence to: jdzak@uic.edu

Abstract

Depression can affect quality of life in several ways, including reduced concentration, motivation, and energy. Olfactory anhedonia in depressed patients results in a decreased attraction to pleasant smells and increased aversion to unpleasant odors. We used the Unpredictable Chronic Mild Stress (UCMS) as an induced-depression model to study olfactory perception and avoidance in mice of both sexes. After inducing a depression-like state, we observed an increased sensitivity to aversive odorants as well as an associated increase in escape behavior in an odorized environment. Previous studies using a similar model of induced depression have demonstrated increased neuroinflammation in brain areas, including the medial prefrontal cortex, but few have explored the effects in olfactory processing centers. We used immunohistochemistry to measure changes in astrocytic activation and microglia in multiple olfactory regions of the brain to further investigate the connection between neuroinflammation and odor hypersensitivity. We found an increase in the number of astrocytes in the medial amygdala, which receives direct input from the accessory olfactory bulb, and more complex microglial morphology in the olfactory bulb and piriform cortex. Additional analysis revealed a relationship between the extent of neuroinflammation and odor aversion. Our findings indicate that glial cells in sensory processing centers are sensitive to stress-induced depression and contribute to altered olfactory perception.

Introduction

Depression, a common mental disorder affecting around 3.8% of the world population, is generally associated with symptoms such as low concentration, self-deprecating thoughts, and changes in appetite (WHO, 2023). While the cause of depression is influenced by an individual's biology, environmental factors also play a significant role in dictating the severity and symptomatic expression of the disorder (Agid et al., 2000; Baumeister et al., 2014). Consistent subjection to environmental stressors, especially in early life, can put patients at an elevated risk for developing depressive disorders (Baumeister et al., 2014). Depressed individuals often find it difficult to regularly function within society, and anhedonia is a key consideration in the diagnosis of depression, with more severe levels of anhedonia being correlated with more severe depressive episodes (Wu et al., 2025). Symptoms of depression reflect perceptual and cognitive changes and ultimately can affect the ability to function at basic biological levels.

Olfactory anhedonia has been documented in depressed patients, manifesting as lower affinity towards stereotyped pleasant odorants, and increased aversion to unpleasant odors (Atanasova et al., 2010; Kamath et al, 2018; Naudin et al., 2012). Depending on the severity of symptoms, depression can also be accompanied by changes in odorant discrimination ability and a correlated reduction in the size of the olfactory bulbs (Naudin et al., 2012; Negoias et al., 2010; Pabel et al., 2018). Depressive disorders can drastically alter how a person experiences the world; understanding the basis of how depression can affect fundamental sensory function will promote different perspectives on clinical treatment.

Prior work has identified that depression causes an inflammatory response. Chronic stress-induced depression has specifically been shown to decrease neurogenesis, increase cortisol levels, and induce the activation of glial cells (Blossom et al., 2020; Du Preez et al., 2021; Li et al., 2015; Rahimian et al., 2024). In the context of neuroinflammation, astrocytes and microglia have been recognized for their contribution to stress-induced depression (Farooq et al., 2012; Guo et al., 2022). Depression treatments targeting the activation of microglia, for instance, demonstrate that microglia themselves critically contribute to depressive behavior (Tabassum et al., 2022).

In addition to mediating neuroinflammation, astrocytes and microglia also play a role during normal olfactory processing (De Saint Jan and Westbrook, 2005; Reshef et al., 2017; Duan et al., 2020; Wallace et al., 2020; Ung et al., 2021; Gómez-Sotres et al., 2024). Astrocytes in the olfactory bulb glomerular and external plexiform layers regulate odor-evoked excitability via Na^+/K^+-ATPase–mediated K^+ clearance and CB_1 receptor–dependent endocannabinoid signaling, shaping mitral/tufted cell output and chemosensory processing (Bellot-Saez et al., 2017; Gómez-Sotres et al., 2024). In the amygdala, astrocytes modulate the integration of socio-chemosensory information by regulating extracellular neurotransmitter clearance and gliotransmitter-mediated synaptic modulation (Noriega-Prieto et al., 2014). These actions influence excitability and plasticity within circuits receiving olfactory bulb–derived inputs and shape neural representations that guide odor-driven behaviors (Martin-Fernandez et al., 2017; Yang et al., 2025).

On the other hand, microglia participate in neurogenesis within the olfactory bulb by inducing phagocytosis of adult neurons and their dendrites (Lazarini et al., 2012; Denizet et al., 2016). While other studies have established these glial cells' roles in neuroinflammation caused by stress-induced depression in brain regions such as the hippocampus and prefrontal cortex (Blossom et al., 2020; Du Preez et al., 2021), little is known about how they modulate sensory processing in response to depressive states, especially in the context of olfaction.

We therefore investigated how exposure to chronic stress can affect behavioral responses to odorants and further explored the prevalence and morphology of astrocytes and microglia in various olfactory brain regions.

Materials and Methods

Animals

Twenty-three adult male and female C57Bl6/J mice were used in this study and were randomly sorted into the control group (*n* = 11) or the stressed group (*n* = 12). Both groups were housed in groups of 3-4 in standard laboratory cages (19 cm x 30 cm x 13 cm) at the University of Illinois Chicago Biological Research Laboratory. All mice experienced a 12-hour light/dark cycle at a temperature of 22 ± 2 ºC and had access to food and water *ad libitum* except during the Restraint stressor (**Table 1**).

Ethics Oversight.

All experiments were performed in accordance with the guidelines set by the National Institutes of Health and approved by the Institutional Animal Care and Use Committee at the University of Illinois Chicago (protocol 24-167).

Unpredictable Chronic Mild Stress (UCMS)

Stressed mice were subjected to a series of different mild stressors five days a week for four consecutive weeks. Stressed animals were subjected to one mild stressor per day for four consecutive hours. All stress procedures were performed during the light cycle in a different room from the housing room. Detailed descriptions of the stressors used are in **Table 1**. The order of the stressors was randomized to maintain unpredictability. The experimental schedule for the UCMS model is outlined in **Table 2**. For stressors involving water, the water was kept at a stable, warm temperature (30 ºC). Afterwards, mice were placed into a heated recovery cage and returned to their home cage after rejuvenation.

Table 1. UCMS protocol stressors

Stressor	Description
Social stress	Mice are placed into a cage that has been previously occupied by another group of mice of the opposite sex for at least two days.
Wet cage	A cage without bedding or enrichment was filled 1 cm deep with water.
Dampened bedding	200 mL of water was added for every 100 g of bedding.
Empty cage	Cage with no bedding, or enrichment.
Titled cage	Cage was tilted at 45º.
Restraint	Mice are placed in a restraining device that prevents movement but still allows access for respiration and air circulation.

Table 2. UCMS protocol schedule

	Day 1	Day 2	Day 3	Day 4	Day 5
Week 1	Social stress	Wet cage	Dampened sawdust	Empty cage	Wet cage
Week 2	Tilted cage	Empty cage	Restraint	Dampened sawdust	Tilted cage
Week 3	Social stress	Wet cage	Restraint	Empty cage	Dampened sawdust
Week 4	Tilted cage	Wet cage	Empty cage	Social stress	Restraint

Behavioral Assessments

Both the control and stressed groups of mice experienced each behavioral assessment. Testing occurred during the light phase, between 8 AM and 2 PM, in a room separate from the housing room. After habituation to each assessment arena, testing occurred one week before and one week after the stressed group experienced UCMS, as outlined in **Figure 1**, and the schedule for these tests is outlined in **Table 3**.

Table 3. Sample behavioral schedule. These tests were performed over the course of one week before implementing the UCMS protocol and were performed once more after the UCMS protocol. The odorant used was either Trimethylamine or Isopentylamine (see *Light/dark Box Odor Aversion Test* for details).

	Day 1	**Day 2**	**Day 3**	**Day 4**	**Day 5**
Behavioral Assessment	Light/dark Box Aversion Test (no odorant, 0%) Tail Suspension Test	Forced Swim Test	Light/dark Box Aversion Test (0.1% concentration)	Light/dark Box Aversion Test (1% concentration)	Light/dark Box Aversion Test (10% concentration)

Forced Swim Test

A clear glass cylinder (30 cm x 15 cm x 15 cm) was filled to 15 cm with room temperature (23-25 ºC) water. Mice were placed at a random point in the water and left to swim for 6 minutes. Videos of each session were scored manually by noting the amount of time the mouse spent immobile in the water. The first two minutes of the session were habituation, and only the last four minutes were scored. Raw scores in seconds were normalized using ((value - minimum) / range) and displayed as the Immobility Score. Statistical comparisons were computed in MATLAB using the rank-sum test for unpaired samples and the signed-rank test for paired samples. Data are given as mean ± standard error of the mean (SEM).

Tail Suspension Test

Mice were suspended at a height of about 20-25 cm using lab labeling tape 3-4 cm form the base of the tail. Plastic cylinders were placed around the mouse's tail to prevent tail climbing behavior. Videos of each six-minute session were scored manually by noting the amount of time the mouse spent motionless in the air. The full six minutes of the session were scored. Raw scores in seconds were normalized using ((value - minimum) / range) and displayed as the Immobility Score. Statistical comparisons were done using the rank-sum test for unpaired samples and the signed-rank test for paired samples. Data are given as mean ± SEM.

Open Field Test

An opaque 51 cm x 56 cm x 16 cm arena was used for behavioral assessment, and a clear acrylic board was placed over the arena to prevent escape and allow for video recording. Mice were consistently placed in the same corner of the arena and allowed to freely roam for 10 minutes. The arena was cleaned with 70% ethanol between animals. Behavior was recorded using the software IC Capture at 10 frames per second using a USB camera (DFK 42BUC03, The Imaging Source) with an accessory camera lens (IP/CCTV 13VM308ASIRII, Tamron). Videos were further processed with ImageJ (Schindelin et al., 2012) and custom MATLAB scripts that measured the mouse's location from the midpoint of its body and tracked the mouse's location and average velocity within the arena. Statistical comparisons were done using the rank-sum test for unpaired samples and the signed-rank test for paired samples. Data are displayed as mean ± SEM.

Odorized Light/Dark Box Test

The behavior apparatus consisted of two 18 cm x 30 cm x 12 cm chambers connected by a 6 cm diameter tube. The light chamber was semi-transparent, while the dark chamber was covered with black acrylic paint. The dark chamber had two air inlets that allowed both air and odor to flow into the chamber at a constant rate of <100 mL/min. The apparatus was placed in a larger sound and light-proof chamber that was lit with LED lights. During testing, an opaque board was placed on top of the dark chamber to further dim the inside of the dark chamber, and a clear acrylic board was placed over the entire apparatus to keep both mice and odor within the chambers, as well as to allow for video recording. Mice were initially placed into the dark chamber and allowed to explore the apparatus for five minutes, at which point the air inlet in the dark chamber was switched to the odor inlet. Trimethylamine (CAS: 75-50-3, Sigma Aldrich) and isopentylamine (CAS: 107-85-7, Sigma Aldrich) were serially diluted into three concentrations using mineral oil. For sessions in which no odor was used, the air inlet was not switched. Sessions lasted for a total of 10 minutes, and the order of individual mice was randomized. One session for each mouse was held per day, and the odor concentration increased the following day. The apparatus was cleaned with 70% ethanol and vacuumed for at least 5 minutes after each session to clear the chambers of the introduced odor and any social cues left behind by the previous mouse.

Only behavior from the light chamber was recorded. Behavior videos were recorded and processed in ImageJ as previously described. Custom MATLAB codes measuring the mouse's location from the midpoint of its body were used to calculate the amount of time spent in each chamber. The percent change was calculated as ((portion of time spent in the dark chamber after the UCMS protocol - portion of time spent in the dark chamber before the UCMS protocol) / portion of time spent in the dark chamber before the UCMS protocol) * 100. Statistical analysis was done using the rank-sum test and two-way analysis of variance (ANOVA). Values are given as mean ± SEM.

Perfusion and Immunohistochemistry

Both control and stressed groups were anesthetized with a ketamine/xylazine solution (100 mg/10 kg) via intraperitoneal injection. The degree of anesthetization was verified via toe pinches before transcardial perfusion with 10 mL of phosphate-buffered saline, followed by 10 mL of 10% formalin. Brains from both control and stressed experimental groups were fixed overnight in 4 mL of formalin, then dehydrated in a 30% sucrose solution for at least 72 hours before sectioning. Brains were suspended in Optimal Cutting Temperature compound for cryosectioning with a Leica CM1800 cryostat at 40 μm thickness. Sections were stored at 4 ºC in phosphate-buffered saline (PBS) until immunohistochemistry was performed.

For immunohistochemistry, 9-11 brain sections were collected from each animal. Sections were chosen based on the presence of the following regions of interest: glomerular and granule cell layer of the main olfactory bulb, the accessory olfactory bulb, the anterior olfactory nucleus, the piriform cortex, and the medial amygdala. These sections were washed for 30 minutes in KPBS with 5-minute interval changes. The tissue then underwent blocking and permeabilization (KPBS with 0.3% Triton-X 100 and 2% donkey serum) for 30 minutes. After washing once more in KPBS for 20 minutes with 5-minute interval changes, the tissue was incubated in rabbit anti-Iba1 (1:100, Fujifilm, catalog number 019-19,741) and placed on an orbital platform overnight at room temperature. The tissue was washed again in KPBS for 30 minutes with 5-minute interval changes and incubated in goat anti-GFAP (1:100, Abcam, catalog number AB_53554) on an orbital platform, again overnight at room temperature. After washing for 40 minutes in KPBS at 5-minute intervals, the tissue was incubated in secondary antibodies anti-RB-TRITC and anti-GT-FITC (1:500, Jackson Immuno Research, catalog number 705-095-003) in antibody diluent (1x KPBS, 0.02% sodium azide, 2% donkey serum). The tissue was washed for 30 minutes in KPBS with 5-minute change intervals and mounted on glass slides using ProLong Gold Antifade with DAPI (Invitrogen, catalog number P36931). Slides were stored at 4 ºC until imaging.

Image analysis for microglia and astrocytes

Images were obtained using a Zeiss LSM800 confocal microscope at 10x or 25x for particle or Scholl analysis. These images were captured semi-randomly as 10-20 plane Z-stacks (Z-interval = 1 μm), with the only requirements being that they were taken within the previously listed regions of interest and that at least one full microglia and astrocyte was centered within the stack. For each region of interest (ROI), three images were taken from two different tissue sections for each animal. 3-4 animals were used for each experimental group.

For astrocytes, each 25x Z-stack image was processed in ImageJ. The image was split into separate color channels before being collapsed into a maximum-intensity projection. An image threshold was then set using the default parameters upon selecting the threshold type "Otsu." After setting the threshold, Fiji's "analyze particles" function was used with the pixel size set as 15-infinity. The "Count" output was taken into consideration for analysis, and a two-tailed rank-sum test was conducted to compare astrocyte counts between groups for each ROI. A total of 10-20 images were used per ROI for each experimental group.

For microglia, 25x Z-stack images were processed in ImageJ. The image was collapsed into a maximum-intensity projection and then split into different color channels. From the maximum-intensity projection, random spatially isolated microglia were outlined with a freehand region of interest (ROI) by lab members blinded to the experimental condition. The surrounding area was removed using ImageJ's "clear outside" function, and an image threshold was set using the default parameters of the "Default" threshold type. An ROI was then indicated at the center of the soma, the single microglia mask was skeletonized using ImageJ's "skeletonize" plugin, and a Scholl analysis was performed using the Fiji Scholl tool with the following parameters: start radius (from the center of the indicated ROI at the soma) = 3 μm, step size = 2 μm, and end radius = 50 μm. The number of identified intersections at each 2 μm step for each microglia measured from each animal was taken into consideration for analysis. A two-way ANOVA was performed to compare the number of intersections at each 2 μm step between groups for each ROI, and interpretation of the results was adjusted with a Bonferroni correction. A total of 18 microglia were measured from each experimental group for each ROI specified previously.

Results

Unpredictable stressors induce a depressive-like state in mice

We developed a standardized protocol (see *Methods*) consisting of six mild, but unpredictable stressors (UCMS) to induce a depressive-like state in adult male and female mice. Recent studies have also used a similar design to study habit formation in the context of stress (Giovanniello et al., 2025). Our panel of stressors and the unpredictability of their implementation resulted in a cumulative effect that gave rise to behavioral phenotypes that are characteristic of depression-like symptoms in rodent models (Mineur et al., 2007; Kreisel et al., 2014).

We began our study by first validating the efficacy of our approach. From each animal, we first collected baseline measurements of immobility using two standard behavioral assays, the Forced Swim Test and the Tail Suspension Test (see *Methods*; **Figure 1A**). Animals were then randomly divided into either a stress group and exposed to the UCMS protocol, or a control group that received equivalent daily handling. After four weeks, mice were then reassessed for immobility on both the Forced Swim Test and the Tail Suspension Test. During the initial Forced Swim Test, there was no difference in the immobility scores (defined as the fraction of time spent actively swimming) between the control and stressed groups (0.4300 ±0.0648 in control animals, n = 11 and 0.3534 ±0.0221 in stressed animals, n = 12; p = 0.4060, rank-sum test; **Figure 1B**; **Table 4**). However, following four weeks of UCMS, the stressed group showed a reduction in their immobility score from baseline measurements (0.3534 ± 0.0221 before stressors and 0.1513 ± 0.0189 after stressors, n = 12; $p = 4.8828 \times 10^{-4}$, signed-rank test; Bonferroni corrected critical

value = 0.0125; **Figure 1B**; **Table 4**), indicating less time attempting to swim in the chamber. A reduction in swimming time has been observed in other studies of learned helplessness and depression in rodents (Yankelevitch-Yahav et al., 2015; Kraeuter et al., 2019). In the control group, there was no difference in the immobility scores following four weeks of daily handling with no stressors (0.4300 ± 0.0648 before stressors and 0.1513 ± 0.0189 after stressors, n = 11; p = 0.0322, signed-rank test; Bonferroni corrected critical value = 0.0125; **Figure 1B**; **Table 4**).

The Tail Suspension Test similarly showed no difference between groups in the amount of time spent immobile prior to UCMS (0.5072 ± 0.0305 in control animals, n = 11, and 0.5068 ± 0.0409 in stressed animals, n = 12; p = 0.8294, rank-sum test; **Figure 1C**; **Table 4**). Following UCMS, the stressed group showed reduced time struggling (0.5068 ± 0.0409 before stressors and 0.2092 ± 0.0428 after stressors, n = 12; $p = 4.8828 \times 10^{-4}$, signed-rank test; Bonferroni corrected critical value = 0.0125; **Figure 1C**; **Table 4**), while there was no difference in the control group after daily handling (0.5072 ± 0.0305 before stressors and 0.4382 ± 0.0797 after stressors, n = 11; p = 0.3203, signed-rank test; Bonferroni corrected critical value = 0.0125; **Figure 1C**; **Table 4**).

As a final test, to ensure that UCMS did not result in generalized motor deficits, which could manifest as a reduction in struggle behavior, we measured the locomotor activity of each mouse in an open field arena. In both groups, after the UCMS protocol, there was no difference in their normalized mean velocity and total movement as they traversed the arena (10.8299 ± 0.9064 cm/s before stressors and 11.5830 ± 1.2488 cm/s after stressors in the control group, p = 0.7002, n = 11, signed-rank test; 11.4210 ± 0.6032 cm/s before stressors and 13.6825 ± 0.7658 cm/s after stressors in the stressed group, p = 0.0923, n = 12, signed-rank test; **Figure 1D**; **Table 4**). Because the observed behavioral alterations occurred in the absence of motor impairments, this suggests that UCMS selectively alters affective state rather than general activity levels (Mineur et al., 2006; Antoniuk et al., 2019). These results demonstrate that our four-week paradigm of daily unpredictable mild stressors is sufficient to induce depressive-like behaviors in mice, resulting in a reduction of self-preservation behaviors.

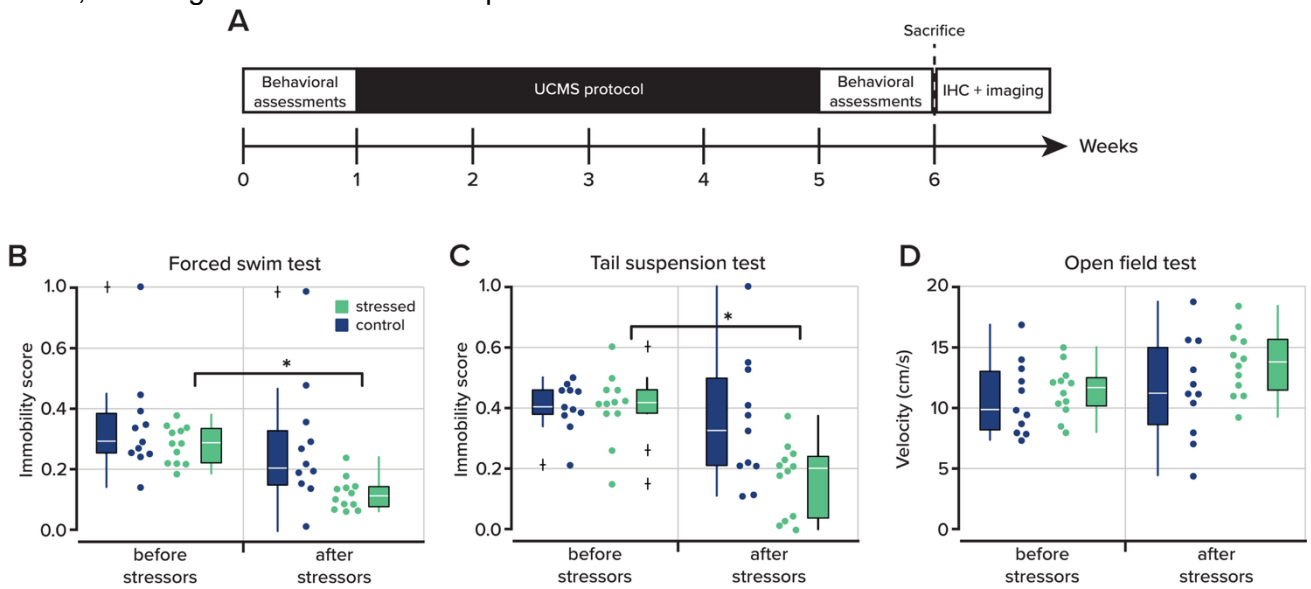

Figure 1. Stress induces a depressive-like state in mice.
A. Experimental timeline of the UCMS protocol and the behavioral assessments. At the end of the behavioral assessments after UCMS, mice were sacrificed for immunohistochemistry. **B.** The immobility score (see *Methods*) in the Forced Swim Test for the control (n = 11) and stressed (n = 12) groups from before and after exposure to the UCMS protocol stressors ($p = 4.883 \times 10^{-4}$, signed-rank test). **C.** The immobility score in the Tail Suspension Test before and after exposure to stressors ($p = 4.883 \times 10^{-4}$, signed-rank test). **D.** Open Field Test results plotted as the mean velocity of experimental groups before and after exposure to UCMS. Dots represent experimental replicates. The white line in the box represents the median, the box edges indicate the 25th and 75th percentiles, respectively. The whiskers extend to the most extreme data points. Outliers are plotted individually using the '+' marker symbol.

Table 4. Figure 1 statistics

Behavioral Test	Comparison	*p*-value	*z*-statistic	*n*	Statistical Test
Forced Swim Test	Control-Control before and after stressors	0.0329	2.1339	11	signed-rank
	Stressed-Stressed before and after stressors	4.8828×10^{-4}	3.0594	12	signed-rank
	Control-Stressed before stressors	0.4060	0.8309	11 control 12 stressed	rank-sum
	Control-Stressed after stressors	0.0151	2.4311	11 control 12 stressed	rank-sum
Tail Suspension Test	Control-Control before and after stressors	0.2860	1.0669	11	signed-rank
	Stressed-Stressed before and after stressors	4.8828×10^{-4}	3.0594	12	signed-rank
	Control-Stressed before stressors	0.8294	-0.2154	11 control 12 stressed	rank-sum
	Control-Stressed after stressors	0.0337	2.1233	11 control 12 stressed	rank-sum
Open Field Test	Control-Control before and after stressors	0.7002	-0.4446	11	signed-rank
	Stressed-Stressed before and after stressors	0.0923	-1.7258	12	signed-rank
	Control-Stressed before stressors	0.4060	-0.8309	11 control 12 stressed	rank-sum
	Control-Stressed after stressors	0.2301	-1.2001	11 control 12 stressed	rank-sum

Bonferroni corrected critical value = 0.025

Tolerance of aversive olfactory stimuli is decreased following exposure to stressors

We next wanted to understand how depressive-like states may influence both tolerance and aversion of olfactory stimuli. We hypothesized that the depressive-like state conferred by UCMS would render mice more sensitive to aversive olfactory stimuli.

We devised a behavioral paradigm that consisted of two chambers connected by a tunnel. One chamber was transparent and illuminated, while the other was made completely opaque and darkened. Mice were allowed to freely explore the apparatus for five minutes, after which the darkened chamber was odorized using air inlets. Odorants were delivered to a carrier stream so that air was constantly flowing to the dark chamber for the duration of the experiment (**Figure 2A**). Earlier work characterizing mouse behavior preferences for illuminated and darkened chambers revealed that mice prefer to spend the majority of their time in the darkened chambers (Costall et al., 1989). This allowed us to ask how odor quality and aversion can be balanced with the relative “safety” of the dark environment.

We tested two separate odorants known to have aversive qualities to mice, trimethylamine and isopentylamine (Belonio et al., 2025; Root et al., 2014), but that are not associated with predator cues. Mice were tested across a range of concentrations for both odorants (0% - 10% v/v for trimethylamine and 0% - 1% v/v for isopentylamine). The amount of time spent in the darkened chamber was then compared to the pre-odor period and calculated as a percent change. For both odorants, we found that the stressed group spent less time in the odorized chamber than the control group (**Figure 2B**,**C**). At the highest concentration (10% v/v) of trimethylamine, the stressed group spent 51.3260 ± 15.9051% (n = 8) less time in the darkened odorized chamber compared to 12.6859 ± 6.7897% (n = 7) less time in the control group (p = 0.0289; z-statistic = 2.1410; rank-sum test). When we considered the behavioral aversion of both groups at all odorant concentrations, there was a difference between the stressed and

control group, with the stressed group more strongly avoiding the odorized compartment (p = 0.0020; $F_{(3,1)}$ = 5.7300; two-way ANOVA; **Figure 2B**). A similar relationship was found when we used the odorant isopentylamine; the stressed group spent less time in the odorized compartment (p = 0.0250; $F_{(2,1)}$ = 8.8300; two-way ANOVA; **Figure 2B**).

Together, our results indicate that, in our induced-depression model, mice show an increased sensitivity and a decreased tolerance of aversive odorants. This was apparent as stressed mice were more willing to leave the relative safety of the darkened chamber when it became odorized.

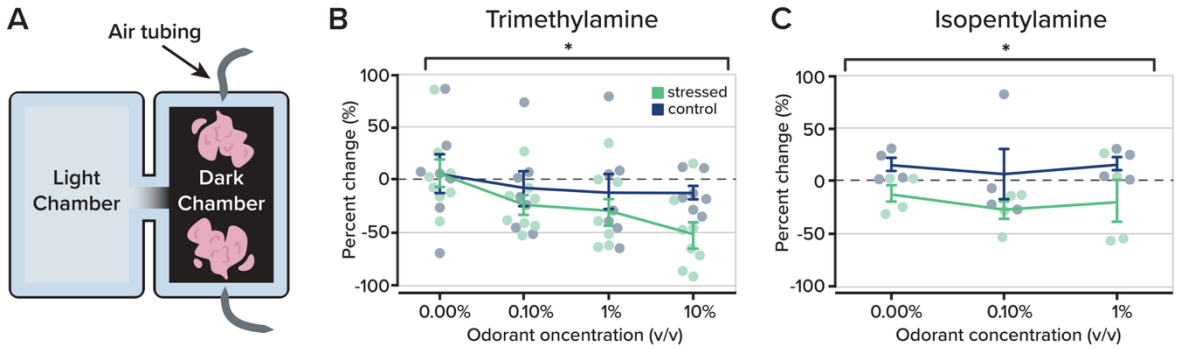

Figure 2. Changes in olfactory-guided behavior in an odorized Light/Dark Box Test.
A. Odorized Light/Dark Box apparatus set up. Odorants trimethylamine and isopentylamine were introduced in the dark chamber at different concentrations using v/v dilutions (0%, 0.1%, 1%, 10%). **B.** Behavioral response to introduction of odorant trimethylamine plotted as percent change (%) of the time spent in the dark chamber from before and after exposure to the UCMS protocol between the control (n = 7) and stressed (n = 8) groups. A difference was found across all odorant concentrations using a two-way ANOVA test with repeated measures: $F_{(3,1)}$ = 5.7300, p = 0.0020. A rank-sum test revealed a difference between groups at 10% concentration, p = 0.0289. **C.** Similar to *part B*, behavioral response to the odorant isopentylamine is plotted to visualize comparisons between control (n = 4) and stressed (n = 4) groups. A two-way ANOVA with repeated measures revealed a difference between experimental groups across all concentrations: $F_{(2,1)}$ = 8.8300, p = 0.0250. Data are displayed as mean ± SEM. Individual dots represent experimental replicates.

Neuroinflammatory markers associated with chronic stress

Neuroinflammation is a biomarker of chronic stress and is also associated with depression (Troubat et al., 2021; Guo et al., 2023). Among the primary cellular mediators of neuroinflammation are astrocytes, which become reactive under pathological conditions and exhibit upregulation of glial fibrillary acidic protein (GFAP), a hallmark of astrogliosis. To assess whether UCMS elicited neuroinflammatory responses in olfactory and limbic brain regions, we examined astrocyte activation across multiple areas known to process odor information and emotional valence.

Following the completion of behavioral testing, brain tissue was stained for GFAP (see *Methods*; **Figure 3A**). We quantified GFAP-positive astrocytes as a readout of glial activation in both primary sensory and higher-order olfactory regions, as well as in the medial amygdala, a region implicated in both olfactory processing and emotional regulation.

At the first stages of sensory processing, in the olfactory bulb and accessory olfactory bulb, we found no difference (**Table 5**) in the number of activated astrocytes (**Figure 3C-H**) between the control and stressed cohorts. Similarly, in the olfactory cortex, the piriform cortex, and the anterior olfactory nucleus, there was also no difference in the total number of GFAP-positive astrocytes. However, in the medial amygdala, which receives olfactory input and also encodes affective state, we found more activated astrocytes in the stressed group than in their non-stressed counterparts (51.2778 ± 6.4731 astrocytes

per imaging field in the control group and 65.0556 ± 4.5045 in the stressed group; n = 18 imaging fields (six imaging fields from three mice in each group); p = 0.0367; rank-sum test). Our findings indicate that repeated stressors drive neuroinflammation in the form of activated astrocytes at loci that receive convergent input from both affective and sensory areas.

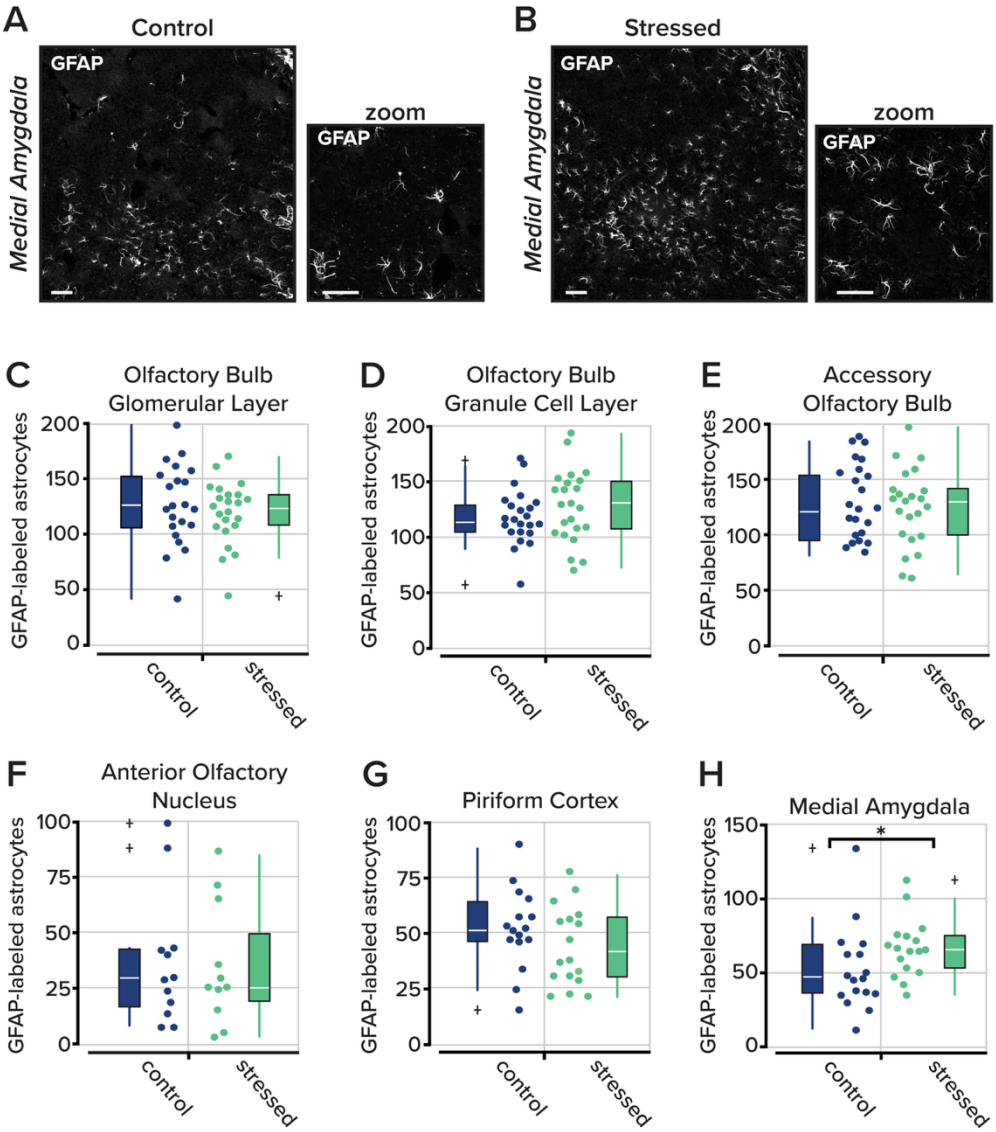

Figure 3. GFAP-labeled astrocytes throughout the olfactory system.
A. Representative images of astrocytes labeled with GFAP in the medial amygdala at 10x (*left*) and 40x (*right*). Scale bar denotes 50 µm. **B.** Same as *part A* for an animal that underwent the UCMS protocol. **C-H.** The total number of GFAP-labeled astrocytes counted in different regions of interest: the olfactory bulb glomerular layer, olfactory bulb granule cell layer, accessory olfactory bulb, anterior olfactory nucleus, piriform cortex, and medial amygdala. In the medial amygdala, a difference between groups was revealed with the rank-sum test (p = 0.0377). Dots represent experimental replicates. The white line in the box represents the median, the box edges indicate the 25th and 75th percentiles, respectively. The whiskers extend to the most extreme data points. Outliers are plotted individually using the '+' marker symbol. n = 3-4 animals per group, three images were analyzed per region of interest.

Table 5. Figure 3 statistics

Location	Control mean ± SEM	Stressed mean ± SEM	*p*-value	*z*-statistic	*n*	Statistical Test
Olfactory bulb glomerular layer	128.5417 ± 7.0446	120.3750 ± 5.5157	0.4641	0.7321	24 each group	rank-sum
Olfactory bulb granule cell layer	114.6667 ± 4.8138	126.7917 ± 6.3591	0.1488	-1.4438	24 each group	rank-sum
Accessory olfactory bulb	126.0000 ± 6.9091	124.1667 ± 7.0149	0.9179	0.1031	24 each group	rank-sum
Anterior olfactory nucleus	36.8333 ± 8.3065	33.5833 ± 7.4706	0.6647	0.4334	12 each group	rank-sum
Piriform Cortex	51.8889 ± 4.0736	44.6111 ± 4.3447	0.3187	0.9971	18 each group	rank-sum
Medial amygdala	51.2778 ± 6.4731	65.0556 ± 4.5045	0.0367	-2.0888	18 each group	rank-sum

Stress induces microglial remodeling in the olfactory system.

In many neurodegenerative disease models, microglia decrease the complexity and size of their processes (Davalos et al., 2005; Qin et al., 2023; Fyke et al., 2024). However, under chronic inflammatory conditions, microglia can develop hypertrophic morphologies (Hains and Waxman, 2006; Loane et al., 2014; Calcia et al., 2016). To test whether our model of induced depression was sufficient to induce microglial activation and morphological changes, we immunostained the same animals for ionized calcium-binding adaptor molecule 1 (Iba1), a protein enriched in microglia and other macrophages (Ito et al., 1998). In images from the same olfactory areas as previously described, we isolated individual microglia and measured the complexity of the processes using a Scholl analysis (see *Methods*), and we calculated the number of path intersections at each concentric ring centered on the microglial soma.

From three mice in each group, we selected two images from each olfactory area. In each image, two microglia were selected by an experimenter blind to the animal condition for further analysis (n = 18 microglia per area in each group). Our results revealed microglial remodeling in two key olfactory structures: the olfactory bulb and piriform cortex. In both regions, microglia from UCMS-treated mice exhibited more complex and extended processes compared to controls (for the glomerular layer of the olfactory bulb: $p = 5.2667 \times 10^{-4}$, for the granule cell layer of the olfactory bulb: $p = 1.8060 \times 10^{-4}$, for the piriform cortex, $p = 7.9000 \times 10^{-6}$; n = 36; Bonferroni corrected critical value = 0.0014; two-way ANOVA, **Figure 4A**–**D**,**G**; **Table 6**), indicative of hypertrophic remodeling. Interestingly, no differences were observed in the accessory olfactory bulb, anterior olfactory nucleus, or medial amygdala (p = 0.0650, p = 0.0138, p = 0.4855 for each region listed respectively; n = 36; Bonferroni corrected critical value = 0.0014; two-way ANOVA; **Figure 4E**,**F**,**H**; **Table 6**), suggesting region-specific vulnerability or temporal dynamics of microglial activation in response to chronic stress.

These findings contrast with our earlier observations of astrocyte reactivity, which was largely restricted to the medial amygdala. While astrocytic changes appeared localized, microglial remodeling was more pronounced in early olfactory processing regions, implicating microglia as sensitive responders to stress-related neuroinflammation in sensory circuits. Together, these data suggest that UCMS elicits differential patterns of glial activation, with microglia in the olfactory bulb and piriform cortex exhibiting robust morphological changes consistent with heightened immune surveillance and potential modulation of local circuit function.

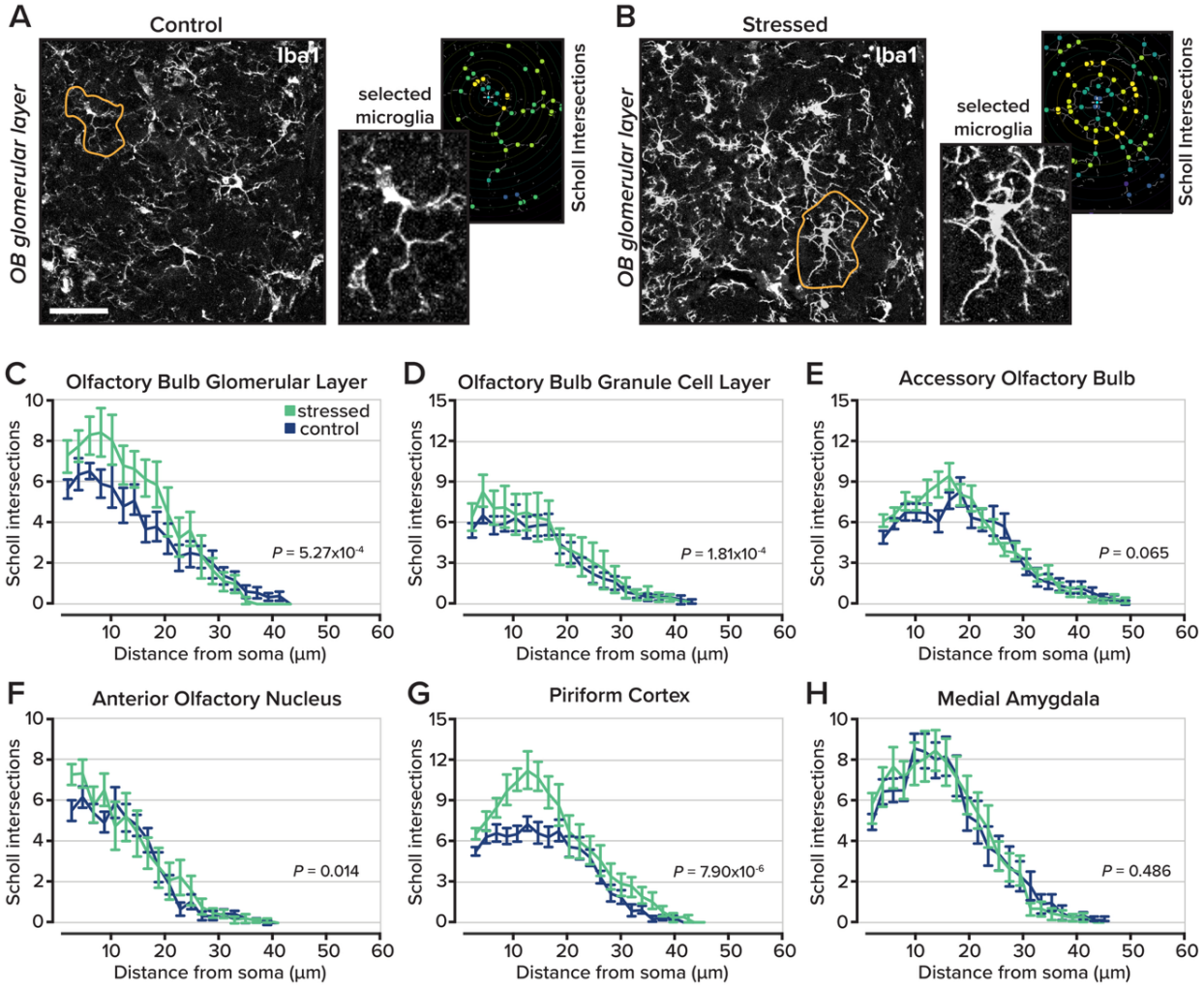

Figure 4. Iba1-labeled microglia in olfactory brain areas.
A. Representative images of microglia labeled with Iba1 in the glomerular layer of the olfactory bulb at 25x. The encircled cell is the cell used for analysis. Scale bar denotes 50 µm. Right, an expanded version of the selected microglia and Scholl intersections. **B**. Same as *part A* for an animal that underwent the UCMS protocol. **C-H.** The number of microglial processes, represented as Scholl intersections, by distance away from the cell soma, in different regions of interest: the olfactory bulb glomerular layer, olfactory bulb granule cell layer, accessory olfactory bulb, anterior olfactory nucleus, piriform cortex, and medial amygdala. The number of Scholl intersections identified in the olfactory bulb glomeruli ($F_{(1,23)} = 16.2132$, $p = 5.27 \times 10^{-4}$), olfactory bulb granule cell layer ($F_{(1,23)} = 19.8565$, $p = 1.806 \times 10^{-4}$), and piriform cortex ($F_{(1,23)} = 32.7587$, $p = 7.900 \times 10^{-6}$) is significant between experimental groups. Statistical tests were performed with a two-way ANOVA. Data are displayed as mean ± SEM. $n = 3$ animals per group, 36 microglia for each region of interest.

Table 6. Figure 4 statistics

Area	F-value	*p*-value	*n*	Statistical Test
Olfactory bulb glomerular layer	(1,23) 16.2132	5.266×10^{-4}	36 each group	two-way ANOVA
Olfactory bulb granule cell layer	(1,23) 19.8565	1.806×10^{-4}	36 each group	two-way ANOVA
Accessory olfactory bulb	(1,23) 3.7544	0.0650	36 each group	two-way ANOVA
Anterior olfactory nucleus	(1,23) 7.112	0.0138	36 each group	two-way ANOVA
Piriform Cortex	(1,23) 32.7587	7.900×10^{-6}	36 each group	two-way ANOVA
Medial amygdala	(1,23) 0.5026	0.4855	36 each group	two-way ANOVA

Behavioral olfactory avoidance is related to neuroinflammation in key olfactory areas

For the final part of our study, we next asked whether behavioral olfactory avoidance was related to the degree of neuroinflammation in each of the olfactory areas we previously analyzed. We identified two areas that demonstrated a relationship between behavioral olfactory avoidance and glial activation: the medial amygdala and the piriform cortex.

In the medial amygdala, we compared the change in time spent in the dark chamber after odorization with 10% trimethylamine and the total number of astrocytes. For our analysis, we considered both cohorts of mice together due to individual variability in both behavior and astrogliosis. Our analysis revealed a relationship between these variables (ρ = -0.3336, T = 2.0600, p = 0.0475, n = 36; **Figure 5A**; **Supplemental Table 1**), thereby indicating that astrocytes in the medial amygdala may play a role in olfactory avoidance. In each of the other areas that we included in our analysis, we found no relationship between the number of astroglia and behavioral outcomes (**Supplemental Figure 1**; **Supplemental Table 1**).

In terms of microglial activation, we found a similar relationship in the piriform cortex. Here, we compared the mean maximum number of Scholl intersections for all microglia in the piriform cortex of each mouse. Again, we found that microglial activation was related to behavioral avoidance of 10% trimethylamine (ρ = -0.4529, T = 2.9610, p = 0.0055; n = 36; **Figure 5B**; **Supplemental Table 2**). We found no relationship between microglial ramifications and olfactory avoidance in other areas (**Supplemental Figure 2**; **Supplemental Table 2**).

Together, these findings suggest that olfactory avoidance behavior is selectively associated with glial activation in distinct brain regions involved in olfactory processing and emotional salience. The absence of similar correlations in other olfactory areas highlights the regional specificity of these effects and suggests that glial activity in the medial amygdala and piriform cortex may uniquely contribute to the neural mechanisms underlying stress-induced changes in olfactory perception and avoidance.

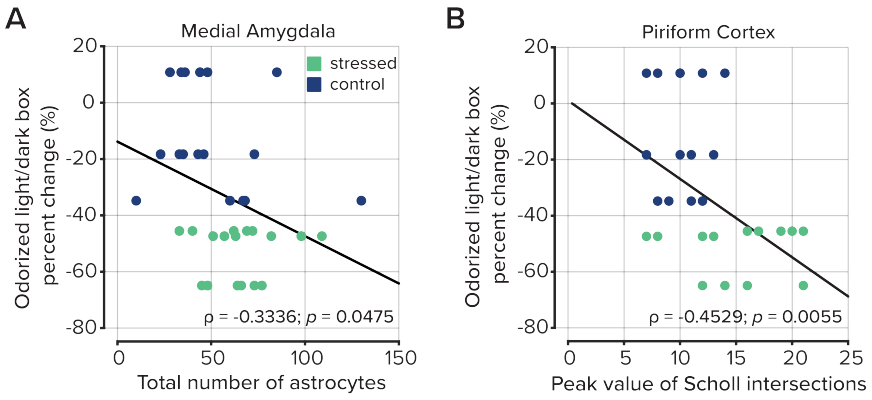

Figure 5. Correlation analysis between inflammatory response and behavior in the Odorized Light/Dark Box Test. **A.** The total number of astrocytes plotted by the percent change of time spent in the dark chamber with the presented odorant. Plotted values represent each animal's results from the behavioral assessment and IHC imaging. *p*-values were determined by calculating the T-value from the linear regression, $p = 0.0475$. **B.** The highest recorded number of intersections identified by Scholl analysis in the microglia sampled by the percent change of time spent in the dark chamber with the presented odorant, $p = 0.0055$.

Discussion

In humans, depression is known to alter olfactory perception, tolerance, and aversion (Lombion-Pouthier et al., 2006; Atanasova et al., 2010; Athanassi et al., 2021). Clinical studies have shown that individuals with major depressive disorder exhibit reduced olfactory sensitivity, decreased hedonic ratings of pleasant odors, and heightened aversion to unpleasant ones (Pause et al., 2001; Lombion-Pouthier et al., 2006; Croy et al., 2014). These alterations are not merely perceptual deficits but are thought to reflect broader disruptions in how affective salience is assigned to sensory stimuli. For example, depressed patients often show diminished approach behavior to rewarding odors and increased withdrawal from aversive odors (Atanasova et al., 2010; Rochet et al., 2018).

Our findings recapitulate depression-induced olfactory sensitivity in a rodent model. UCMS-treated mice displayed a depressive-like state, characterized by increased immobility in the Forced Swim Test and Tail Suspension Test, behaviors commonly used to model learned helplessness and depression (Porsolt et al., 1977; Steru et al., 1985; Willner, 2005). UCMS-treated mice also showed an increased avoidance of odorized environments, even when those environments were otherwise preferred (i.e., dark and enclosed; Costall et al., 1989). This suggests that depressive-like states in mice, like in humans, sensitize individuals to olfactory threats and reduce tolerance for aversive stimuli. Given the strong anatomical and functional links between olfactory and limbic circuits (Soudry et al., 2011; Yao et al., 2020), these data further support the hypothesis that altered olfactory processing in depression arises from disrupted integration between sensory input and emotional valence.

Our findings extend beyond behavioral phenotyping by identifying distinct patterns of neuroinflammatory activation in olfactory and limbic brain regions following UCMS. Astrocytic activation, measured via GFAP expression, was elevated selectively in the medial amygdala, a region implicated in the affective appraisal of sensory stimuli and in the integration of olfactory and emotional information (Swanson & Petrovich, 1998; Janak & Tye, 2015). In contrast, microglial remodeling was observed in primary sensory structures, the olfactory bulb and piriform cortex, where increased process complexity is a known hallmark of chronic stress-induced microglial activation (Kreisel et al., 2014; Calcia et al., 2016). These cell-type- and region-specific differences suggest that astrocytes and microglia may respond to chronic stress via distinct mechanisms that differentially affect sensory and emotional brain circuits (Liddelow et al., 2017; Yirmiya et al., 2015).

In the final part of our study, we found that glial activation in these regions was associated with olfactory avoidance behavior. The number of GFAP-positive astrocytes in the medial amygdala correlated with increased avoidance of aversive odorants, suggesting that astrogliosis in this region may alter affective salience encoding and influence behavioral responses to environmental threats (Tynan et al., 2013; Seo et al., 2016). Similarly, microglial complexity in the olfactory bulb and piriform cortex was correlated with odor avoidance, implicating immune-mediated modulation of primary sensory circuits in the processing of aversive olfactory stimuli (Chen et al., 2016; Füzesi et al., 2016). The absence of similar relationships in other olfactory areas supports the idea of regional specificity in how neuroinflammation affects sensory-driven behavior.

Together, our findings support a model in which chronic stress alters odor perception and behavioral reactivity through glial-mediated remodeling of sensory and affective neural circuits. While previous work has largely focused on neuroinflammation in classic limbic structures such as the hippocampus and prefrontal cortex (Duman et al., 2016; Wohleb et al., 2018), our data highlight the olfactory system as a novel site of stress-sensitive neuroimmune interactions. Future work should examine whether direct manipulation of glial activity in these regions can rescue olfactory deficits or normalize behavioral responses to aversive stimuli. Such interventions may yield novel therapeutic strategies that target glial function to alleviate sensory and affective symptoms in depression.

Acknowledgements

We thank Angie Salles for sharing equipment and resources. The Department of Biological Sciences Imaging Core for microscopy assistance and all members of the Zak Laboratory for helpful discussions throughout this project.

Funding and Support

This work was supported by NIH Grant DC017754 to JDZ.

Competing Interests

The authors declare no competing interests.

References

Agid O, Kohn Y, Lerer B (2000) Environmental stress and psychiatric illness. Biomed Pharmacother 54:135–141.

Atanasova B, El-Hage W, Chabanet C, Gaillard P, Belzung C, Camus V (2010) Olfactory anhedonia and negative olfactory alliesthesia in depressed patients. Psychiatry Res 176:190–196.

Athanassi A, Dorado Doncel R, Bath KG, Mandairon, N (2021) Relationship between depression and olfactory sensory function: A Review. Chem Senses 46.

Baumeister D, Lightman SL, Pariante, CM (2014) The interface of stress and the HPA axis in behavioural phenotypes of mental illness. Curr Top Behav Neurosci 13–24.

Belonio KC, Haile ES, Fyke Z, Vivona L, Konanur V, Tulabandhula T, Zak JD (2025) Amplification of olfactory transduction currents implements sparse stimulus encoding. J Neurosci 45:e2008242025.

Bellot-Saez A, Kékesi O, Morley JW, Buskila Y (2017) Astrocytic modulation of neuronal excitability through K+ spatial buffering. Neurosci Biobehav Rev 77:87–97.

Blossom V, Gokul M, Kumar NA, Kini RD, Nayak S, Bhagyalakshmi K (2020) Chronic unpredictable stress-induced inflammation and quantitative analysis of neurons of distinct brain regions in Wistar rat model of comorbid depression. Vet World 13:1870–1874.

Calcia MA, Bonsall DR, Bloomfield PS, Selvaraj S, Barichello T, Howes OD (2016) Stress and neuroinflammation: a systematic review of the effects of stress on microglia and the implications for mental illness. Psychopharmacology (Berl). 233:1637–1650.

Costall B, Jones BJ, Kelly ME, Naylor RJ, Tomkins DM (1989) Exploration of mice in a black and white test box: Validation as a model of anxiety. Pharmacol Biochem Behav 32:777–785.

Croy I, Nordin S, Hummel T (2014) Olfactory disorders and quality of life--an updated review. Chem Senses 39:185–194.

Davalos D, Grutzendler J, Yang G, Kim JV, Zuo Y, Jung S, Littman DR, Dustin ML, Gan WB (2005) ATP mediates rapid microglial response to local brain injury in vivo. Nat Neurosci 8:752–8.

Denizet M, Cotter L, Lledo PM, Lazarini F (2017) Sensory deprivation increases phagocytosis of adult-born neurons by activated microglia in the olfactory bulb. Brain Behav Immun 60, 38–43.

De Saint Jan D, Westbrook GL (2005) Detecting activity in olfactory bulb glomeruli with astrocyte recording. J Neurosci 25:2917–2924.

Duan D, Zhang H, Yue X, Fan Y, Xue Y, Shao J, Ding G, Chen D, Li S, Cheng H, Zhang X, Zou W, Liu J, Zhao J, Wang L, Zhao B, Wang Z, Xu S, Wen Q, Liu J, Duan S, Kang L (2020) Sensory glia detect repulsive odorants and drive olfactory adaptation. Neuron 108:707-721.e8.

Du Preez A, Onorato D, Eiben I, Musaelyan K, Egeland M, Zunszain PA, Fernandes C, Thuret S, Pariante CM (2021) Chronic stress followed by social isolation promotes depressive-like behaviour, alters microglial and astrocyte biology and reduces hippocampal neurogenesis in male mice. Brain Behav Immun 91:24–47.

Farooq RK, Isingrini E, Tanti A, Le Guisquet AM, Arlicot N, Minier F, Leman S, Chalon S, Belzung C, Camus V (2012) Is unpredictable chronic mild stress (UCMS) a reliable model to study depression-induced neuroinflammation? Behav Brain Res 231:130–137.

Fyke Z, Johansson R, Scott AI, Wiley D, Chelsky D, Zak JD, Al Nakouzi N, Koster KP, Yoshii A (2024) Reduction of neuroinflammation and seizures in a mouse model of CLN1 batten disease using the small molecule enzyme mimetic, N-Tert-butyl hydroxylamine. Mol Genet Metab 143:108537.

Gómez-Sotres P, Skupio U, Dalla Tor T, Julio-Kalajzic F, Cannich A, Gisquet D, Bonilla-Del Rio I, Drago F, Puente N, Grandes P, Bellocchio L, Busquets-Garcia A, Bains JS, Marsicano G (2024) Olfactory bulb astrocytes link social transmission of stress to cognitive adaptation in male mice. Nature Commun 15: 7103.

Guo B, Zhang M, Hao W, Wang Y, Zhang T, Liu C (2023) Neuroinflammation mechanisms of neuromodulation therapies for anxiety and depression. Transl Psychiatry 13:5.

Guo J, Qiu T, Wang L, Shi L, Ai M, Xia Z, Peng Z, Zheng A, Li X, Kuang L (2022) Microglia loss and astrocyte activation cause dynamic changes in hippocampal [^{18}F]DPA-714 uptake in mouse models of depression. Front Cell Neurosci 16:802192.

Hains BC, Waxman SG (2006) Activated microglia contribute to the maintenance of chronic pain after spinal cord injury. J Neurosci 26:4308–4317.

Ito D, Imai Y, Ohsawa K, Nakajima K, Fukuuchi Y, Kohsaka S (1998) Microglia-specific localisation of a novel calcium binding protein, Iba1. Brain Res Mol Brain Res 57:1–9.

Janak PH, Tye KM (2015) From circuits to behaviour in the amygdala. Nature 517:284–292.

Kamath V, Paksarian D, Cui L, Moberg PJ, Turetsky BI, Merikangas KR (2018) Olfactory processing in bipolar disorder, major depression, and anxiety. Bipolar Disorders 20:547–555.

Kraeuter AK, Guest PC, Sarnyai Z (2019) The forced swim test for depression-like behavior in rodents. Methods Mol Biol 1916:75–80.

Kreisel T, Frank MG, Licht T, Reshef R, Ben-Menachem-Zidon O, Baratta MV, Maier SF, Yirmiya R (2014) Dynamic microglial alterations underlie stress-induced depressive-like behavior and suppressed neurogenesis. Mol Psychiatry 19:699–709.

Lazarini F, Gabellec MM, Torquet N, Lledo PM (2012) Early activation of microglia triggers long-lasting impairment of adult neurogenesis in the olfactory bulb. J Neurosci 32:3652–3664.

Li Q, Yang D, Wang J, Liu L, Feng G, Li J, Liao J, Wei Y, Li Z (2015) Reduced amount of olfactory receptor neurons in the rat model of depression. Neurosci Lett 603:48–54.

Liddelow SA, Guttenplan KA, Clarke LE, Bennett FC, Bohlen CJ, Schirmer L, Bennett ML, Münch AE, Chung WS, Peterson TC, Wilton DK, Frouin A, Napier BA, Panicker N, Kumar M, Buckwalter MS, Rowitch DH, Dawson VL, Dawson TM, Stevens B, Barres BA (2017) Neurotoxic reactive astrocytes are induced by activated microglia. Nature 541:481–487.

Loane DJ, Kumar A, Stoica BA, Cabatbat R, Faden AI (2014) Progressive neurodegeneration after experimental brain trauma: association with chronic microglial activation. J Neuropathol Exp Neurol 73:14–29.

Lombion-Pouthier S, Vandel P, Nezelof S, Haffen E, Millot JL (2006) Odor perception in patients with mood disorders. J Affect Disord 90:187–91.

Naudin M, El-Hage W, Gomes M, Gaillard P, Belzung C, Atanasova B (2012) State and trait olfactory markers of major depression. PLOS ONE 7(10).

Negoias S, Croy I, Gerber J, Puschmann S, Petrowski K, Joraschky P, Hummel T (2010) Reduced olfactory bulb volume and olfactory sensitivity in patients with acute major depression. Neuroscience 169:415–421.

Noriega-Prieto JA, Araque A (2011) Sensing and regulating synaptic activity by astrocytes at tripartite synapse. Neurochem Res 46:2580–2585.

Martin-Fernandez M, Jamison S, Robin LM, Zhao Z, Martin ED, Aguilar J, Benneyworth MA, Marsicano G, Araque A (2017) Synapse-specific astrocyte gating of amygdala-related behavior. Nat Neurosci 20:1540–1548.

Mineur YS, Belzung C, Crusio WE (2006) Effects of unpredictable chronic mild stress on anxiety and depression-like behavior in mice. Behav Brain Res 175:43–50.

Mineur YS, Belzung C, Crusio WE (2007) Functional implications of decreases in neurogenesis following chronic mild stress in mice. Neuroscience 150:251–9.

Pabel LD, Hummel T, Weidner K, Croy I (2018) The impact of severity, course and duration of depression on olfactory function. J Affect Disord 238:194–203.

Pause BM, Miranda A, Göder R, Aldenhoff JB, Ferstl R (2001) Reduced olfactory performance in patients with major depression. J Psychiatr Res 35:271–277.

Porsolt RD, Bertin A, Jalfre M (1977) Behavioral despair in mice: a primary screening test for antidepressants. Arch Int Pharmacodyn Ther 229:327–336.

Qin J, Ma Z, Chen X, Shu S (2023) Microglia activation in central nervous system disorders: A review of recent mechanistic investigations and development efforts. Front Neurol 14:1103416.

Rahimian R, Perlman K, Fakhfouri G, Mpai R, Richard VR, Hercher C, Penney L, Davoli MA, Nagy C, Zahedi RP, Borchers CH, Giros B, Turecki G, Mechawar N (2024) Proteomic evidence of depression-associated astrocytic dysfunction in the human male olfactory bulb. Brain Behav Immun. 122:110–121.

Reshef R, Kudryavitskaya E, Shani-Narkiss H, Isaacson B, Rimmerman N, Mizrahi A, Yirmiya R (2017) The role of microglia and their CX3CR1 signaling in adult neurogenesis in the olfactory bulb. Elife 6:e30809.

Rochet M, El-Hage W, Richa S, Kazour F, Atanasova B (2018) Depression, olfaction, and quality of life: A mutual relationship. Brain Sci 8:80.

Root CM, Denny CA, Hen R, Axel R (2014) The participation of cortical amygdala in innate, odour-driven behaviour. Nature 515:269–273.

Schindelin J, Arganda-Carreras I, Frise E, et al. (2012) Fiji: an open-source platform for biological-image analysis. Nat Methods 9:676–82.

Soudry Y, Lemogne C, Malinvaud D, Consoli SM, Bonfils P (2011) Olfactory system and emotion: common substrates. Eur Ann Otorhinolaryngol Head Neck Dis 128:18–23.

Steru L, Chermat R, Thierry B, Simon P (1985) The tail suspension test: a new method for screening antidepressants in mice. Psychopharmacology 85:367–370.

Swanson LW, Petrovich GD (1998) What is the amygdala? Trends Neurosc. 21:323–331.

Tabassum S, Misrani A, Huo Q, Ahmed A, Long C, Yang L (2022) Minocycline ameliorates chronic unpredictable mild stress-induced neuroinflammation and abnormal mPFC-HIPP oscillations in mice. Mol Neurobiol 59:6874–6895.

Troubat R, Barone P, Leman S, Desmidt T, Cressant A, Atanasova B, Brizard B, El Hage W, Surget A, Belzung C, Camus V (2021) Neuroinflammation and depression: A review. Eur J Neurosci 53:151–171.

Ung K, Huang TW, Lozzi B, Woo J, Hanson E, Pekarek B, Tepe B, Sardar D, Cheng YT, Liu G, Deneen B, Arenkiel BR (2021) Olfactory bulb astrocytes mediate sensory circuit processing through Sox9 in the mouse brain. Nat Commun 12:5230.

Wallace J, Lord J, Dissing-Olesen L, Stevens B, Murthy VN (2020) Microglial depletion disrupts normal functional development of adult-born neurons in the olfactory bulb. Elife 9:e50531.

Willner P (2005) Chronic mild stress (CMS) revisited: consistency and behavioural-neurobiological concordance in the effects of CMS. Neuropsychobiology. 52:90–110.

World Health Organization. (2023, March 31). Depressive disorder (depression). World Health Organization. https://www.who.int/news-room/fact-sheets/detail/depression

Wu C, Mu, Q, Gao W, Lu S (2025). The characteristics of anhedonia in depression: A review from a clinically oriented perspective. Transl Psychiatry 15(1).

Yang Q, Zhou G, Sheriff A, Sagar V, Echevarria-Cooper S, Lane G, Kahnt T, Zelano C (2025) The human olfactory amygdala: Anatomical connections between the olfactory bulb and amygdala subregions. Imaging Neurosci 3 imag_a_00571.

Yao Z, Fu Y, Wu J, Zhang W, Yu Y, Zhang Z, Wu X, Wang Y, Hu B (2020) Morphological changes in subregions of hippocampus and amygdala in major depressive disorder patients. Brain Imaging Behav 14:653–667.

Yankelevitch-Yahav R, Franko M, Huly A, Doron R (2015) The forced swim test as a model of depressive-like behavior. J Vis Exp 97:52587.

Yirmiya R, Rimmerman N, Reshef R (2015) Depression as a microglial disease. Trends Neurosci 38:637–658.

Zhao D, Hu M, Liu S (2024) Glial cells in the mammalian olfactory bulb. Front Cell Neurosci 18:1426094.

Supplemental Figures

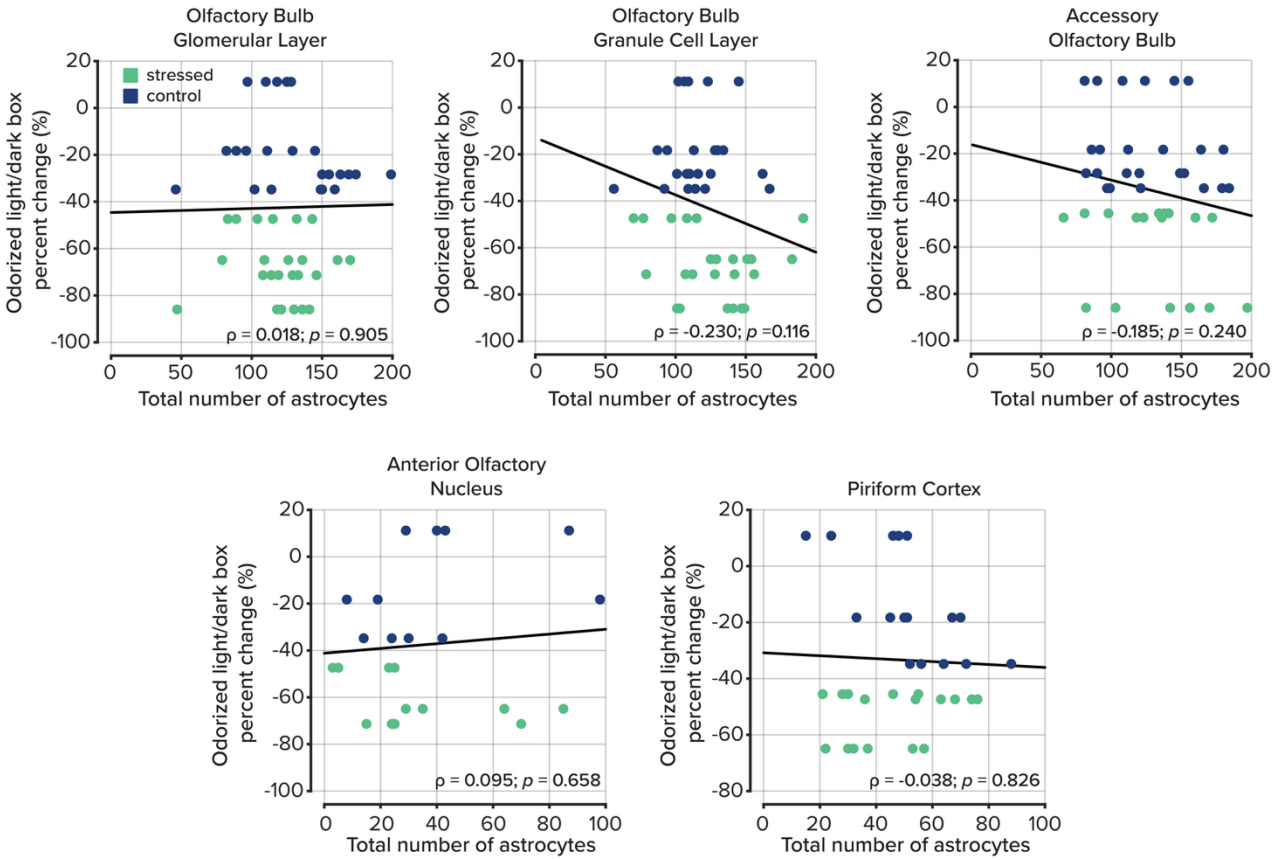

Supplemental Figure 1. Correlation analysis between labeled astrocytes and odorant aversion in the olfactory bulb glomerular layer, olfactory bulb granule cell layer, accessory olfactory bulb, anterior olfactory nucleus, and piriform cortex.

Supplemental Table 1. Summary statistics for correlations between astrocytes and behavioral aversion

Area	ρ-value	T-statistic	*p*-value	*n*
Olfactory bulb glomerular layer	0.0177	0.1200	0.9049	48
Olfactory bulb granule cell layer	-0.2299	1.6045	0.1160	48
Accessory olfactory bulb	-0.1853	1.1865	0.2401	42
Anterior olfactory nucleus	0.0953	0.4470	0.6577	24
Piriform cortex	-0.0380	0.1845	0.8257	36
Medial amygdala	-0.3326	2.0600	0.0475	36

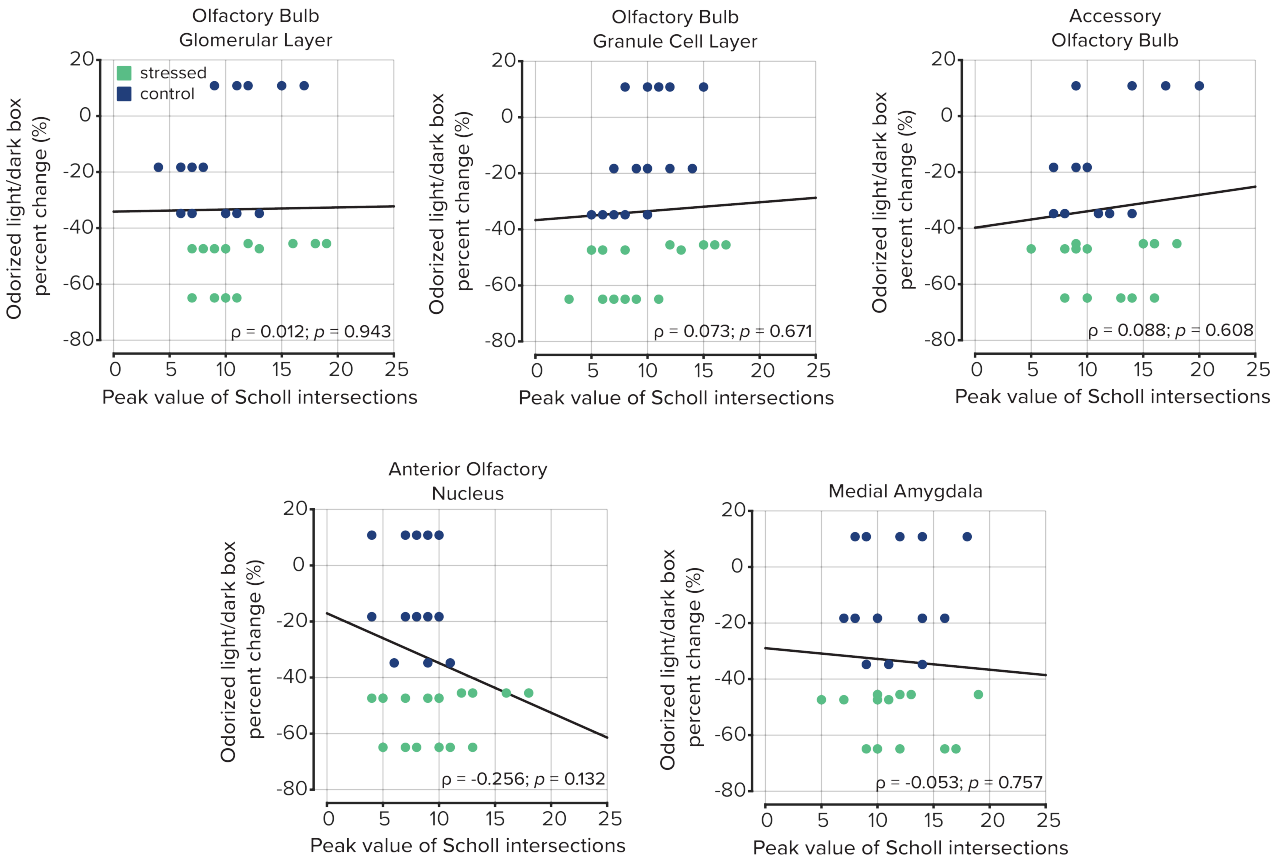

Supplemental Figure 2. Correlation analysis between microglial ramifications and odorant aversion in the olfactory bulb glomerular layer, olfactory bulb granule cell layer, accessory olfactory bulb, anterior olfactory nucleus, and medial amygdala.

Supplemental Table 2. Summary statistics for correlations between astrocytes and behavioral aversion

Area	ρ-value	T-statistic	*p*-value	*n*
Olfactory bulb glomerular layer	0.0123	0.0720	0.9432	36
Olfactory bulb granule cell layer	0.0733	0.4133	0.6709	36
Accessory olfactory bulb	0.0884	0.5236	0.6083	36
Anterior olfactory nucleus	-0.2558	1.5374	0.1321	36
Piriform cortex	-0.4529	2.9610	0.0055	36
Medial amygdala	-0.0534	0.3199	0.7570	36